HHS Public Access

Author manuscript

Nat Methods. Author manuscript; available in PMC 2012 July 01.

Published in final edited form as:

Nat Methods. ; 9(1): 90–95. doi:10.1038/nmeth.1782.

Optical recording of action potentials in mammalian neurons using a microbial rhodopsin

Joel M. Kralj[1,5], **Adam D. Douglass**[2,5], **Daniel R. Hochbaum**[3,5], **Dougal Maclaurin**[4], and **Adam E. Cohen**[1,4]

[1]Department of Chemistry and Chemical Biology

[2]Department of Molecular and Cellular Biology

[3]Applied Physics Program, School of Engineering and Applied Science

[4]Department of Physics, Harvard University, 12 Oxford Street, Cambridge, MA 02138

Abstract

Reliable optical detection of single action potentials in mammalian neurons has been one of the longest-standing challenges in neuroscience. Here we achieve this goal by using the endogenous fluorescence of a microbial rhodopsin protein, Archaerhodopsin 3 (Arch) from *Halorubrum sodomense*, expressed in cultured rat hippocampal neurons. This genetically encoded voltage indicator exhibited an approximately 10-fold improvement in sensitivity and speed over existing protein-based voltage indicators, with a roughly linear two-fold increase in brightness between −150 mV and +150 mV and a sub-millisecond response time. Arch detected single electrically triggered action potentials with an optical signal-to-noise ratio > 10. The mutant Arch(D95N) lacked endogenous proton pumping and showed 50% greater sensitivity than wild-type, but had a slower response (41 ms). Nonetheless, Arch(D95N) also resolved individual action potentials. Microbial rhodopsin-based voltage indicators promise to enable optical interrogation of complex neural circuits, and electrophysiology in systems for which electrode-based techniques are challenging.

Introduction

To study the dynamics of a complex neural circuit, one would like to record action potentials from many neurons simultaneously. Optical imaging promises to realize this goal [1–5], and voltage indicators have been developed based upon small molecules [6, 7],

Correspondence should be addressed to A.E.C. (cohen@chemistry.harvard.edu).

[5]These authors contributed equally to this work

Supplementary Information is available online

Author contributions

AEC conceived the project. JMK, ADD, DRH carried out experiments. DM designed and built the imaging system used in Fig. 2. All authors designed experiments, analyzed data, and wrote the paper.

Competing financial interests

AEC, JMK, and ADD filed a patent application on microbial rhodopsin-based voltage sensors.

fluorescent proteins [8, 9], and hybrid protein-dye systems [10, 11]. Single action potentials with high signal-to-noise ratio were recently recorded in individual spines of mammalian neurons in slice using an organic voltage-indicating dye, but this approach required intracellular injection of dye and cumulative illumination of less than 2 s to avoid phototoxicity [12]. Action potentials in mammalian neurons were recorded *in vivo* using a genetically encoded voltage indicator, but required averaging over multiple trials [4]. Signals suggestive of single spikes were reported when the optical signal was aligned with an electrophysiology trace, but the signal-to-noise ratio was inadequate for all-optical spike identification. Calcium imaging is widely used as an indirect readout of electrical activity, but is only useful where slower readouts (hundreds of ms) are acceptable [13]. Despite this progress, direct and sensitive optical measurement of membrane potential remains elusive. All approaches have one or more serious limitations, including slow response, lack of sensitivity, difficulty in targeting, or phototoxicity. No genetically encoded voltage indicator has had adequate sensitivity and speed to reliably identify action potentials from mammalian neurons on a single-trial basis.

We recently developed a fast and sensitive voltage indicator based on green-absorbing proteorhodopsin [14]. This Proteorhodopsin Optical Proton Sensor (PROPS) revealed electrical spiking in *E. coli*, but efforts to use PROPS in eukaryotic cells failed because the protein did not localize to the plasma membrane. Addition of targeting and localization sequences to PROPS did not help. Thus we decided to test other microbial rhodopsins as putative voltage sensors, focusing on proteins known to localize to the eukaryotic plasma membrane. Archaerhodopsin 3 (Arch) from *Halorubrum sodomense* is a light-driven outward proton pump, capturing solar energy for its host [15]. Recently Arch was expressed in mammalian neurons, wherein it enabled optical silencing of neural activity, and was shown to be minimally perturbative to endogenous function in the dark [16]. We hypothesized that Arch could be run backward: that a membrane potential could alter the optical properties of the protein, and thereby provide a voltage sensor that functioned through a mechanism similar to PROPS.

We found that Arch was capable of resolving individual action potentials in mammalian neurons *in vitro*, with high signal-to-noise ratio and low phototoxicity. Arch enabled mapping of neuronal action potentials with sub-millisecond temporal resolution and sub-cellular spatial resolution. However, the wild-type form of Arch generated a hyperpolarizing photocurrent upon exposure to the imaging laser. The mutation D95N eliminated this photocurrent, but also slowed the response to 41 ms.

Results

Photophysics of Arch

At neutral pH bacterially expressed Arch was pink, but at high pH the protein turned yellow (Fig. 1a), with a pK_a for the transition of 10.1. Based on homology to other microbial rhodopsins [17], we attributed the pH-induced color change to deprotonation of the Schiff base (SB) which links the retinal chromophore to the protein core. We reasoned that a change in membrane potential might change the local electrochemical potential of the proton at the SB, tipping the acid-base equilibrium and inducing a similar color shift. This mechanism of

voltage-induced color shift has previously been reported in dried films of bacteriorhodopsin [18], and formed the hypothesized basis of voltage sensitivity in PROPS [14].

Changes in optical absorption would be challenging to detect in a single cell, due to the small quantity of protein available. However, most microbial rhodopsins are weakly fluorescent [19], so we characterized Arch as a prospective fluorescent indicator (Table 1). At neutral pH, Arch emitted far red fluorescence (λ_{em} = 687 nm), while at high pH Arch was not fluorescent (Fig. 1b, Supplementary Fig. 1). The fluorescence quantum yield of Arch was low (9×10^{-4}) but the photostability was comparable to members of the GFP family [20]. We found that laser illumination and EMCCD detection were necessary for observing Arch fluorescence. A comparison of photobleaching rates of Arch (excited at 640 nm) with eGFP (excited at 488 nm), in a 1:1 Arch-eGFP fusion, showed that the mean numbers of photons emitted per molecule prior to photobleaching were approximately in the ratio 1:3.9 (Arch:eGFP). The broad absorption peak enabled excitation of Arch at λ = 640 nm, a wavelength where few other cellular components absorb, and the far red emission occurred in a spectral region of little background autofluorescence.

Fluorescence of Arch in HEK 293 cells supplemented with 5 μM all-*trans* retinal was readily imaged in an inverted fluorescence microscope with red illumination (λ = 640 nm, 20 mW, I = 540 W cm^{-2}), a high numerical aperture objective, a Cy5 filter set, and an EMCCD camera (Online Methods and Supplementary Fig. 2). The cells exhibited fluorescence predominantly localized to the plasma membrane. Cells not expressing Arch were not fluorescent. Cells showed 17% photobleaching over a continuous 10-minute exposure, and retained normal morphology during this interval.

The fluorescence of HEK cells expressing Arch was highly sensitive to membrane potential, as determined via whole-cell voltage clamp (Supplementary Movie 1). Fluorescence of Arch in the plasma membrane increased by a factor of two between −150 mV and +150 mV, with a nearly linear response throughout this range (Fig. 1c). The response of fluorescence to a step in membrane potential occurred within the 500 μs time resolution of our imaging system on both the rising and falling edge (Fig. 1d). Application of a sinusoidally varying membrane potential led to sinusoidally varying fluorescence; at f = 1 kHz, the fluorescence oscillations retained 55% of their low-frequency amplitude (Supplementary Fig. 3). Arch retained its endogenous proton-pumping capability, and illumination with the imaging laser generated outward photocurrents of 10 –20 pA.

Fluorescent voltage indicators are often characterized by the fractional change in fluorescence, ΔF/F, per 100 mV of membrane potential. This metric suffers from subjectivity in the choice of which pixels are chosen to represent “signal” and which are chosen for “background.” The quantity ΔF/F also does not indicate temporal stability of the signal, nor information about the signal-to-noise ratio (except in the rarely achieved case of shot-noise-limited detection). Thus we sought an objective measure of the precision with which small changes in V_m could be detected.

We developed a linear regression algorithm to identify pixels whose intensity co-varied with an external “training” stimulus (Online Methods and Supplementary Software). When

trained on the unweighted whole-field fluorescence, this algorithm identified pixels associated with the cell membrane (Fig. 1e) and rejected pixels corresponding to bright but voltage-insensitive intracellular aggregates. Application of the pixel weight matrix to the raw fluorescence led to estimates of voltage-induced changes in fluorescence with improved signal-to-noise ratio (SNR) relative to unweighted whole-field fluorescence (Supplementary Software). This use of the pixel weighting algorithm made no use of electrophysiology data.

Fluorescence data alone was insufficient to determine true membrane potential, because cell-to-cell variation in expression level and membrane localization led to an *a priori* unknown offset and scale factor between fluorescence and voltage, which depended on illumination parameters, cell morphology, and expression level. When trained on the electrophysiology data, the algorithm returned pixel weight coefficients that could be used to convert fluorescence images into a maximum likelihood estimate of the membrane potential, $\hat{V_{FL}}$ (Online Methods, Supplementary Software). After training on a voltage sweep from −150 mV to + 150 mV, the fluorescence-based $\hat{V_{FL}}$ matched the electrically recorded V_m with an accuracy of 625 μV $Hz^{-1/2}$ (Supplementary Fig. 4). Over timescales longer than ~10 s, laser power fluctuations and cell motion degraded the sub-mV precision of the voltage determination, but had little effect on the ability to detect fast transients in V_m. Our simple algorithm does not accommodate cell motion, multiple cells undergoing different voltage dynamics, or substantial lags in voltage propagation from one region to another. Other algorithms exist to handle such scenarios however.[21]

Arch fluorescence identifies action potentials in vitro

We tested Arch as a voltage indicator in cultured rat hippocampal neurons, using viral delivery. Neurons expressing Arch showed membrane-localized fluorescence (Fig. 2a). Under whole-cell current clamp, cells exhibited spiking upon injection of current pulses of 200 pA. Individual spikes were accompanied by clearly identifiable increases of whole-field fluorescence (Fig. 2b, Supplementary Movie 2). After scaling of the fluorescence trace to overlay on the voltage, the root-mean-square (r.m.s.) deviation between the two was $\sigma_V \hat{=}$ 7.2 mV. Training the pixel-weighting algorithm on the whole-field fluorescence led to a 74% improvement in SNR, with an r.m.s. error in the predicted voltage (after scaling and offset adjustment) of $\sigma_V \hat{=}$ 4.2 mV (Fig. 2c). This training procedure made no use of the electrical recording. Training the pixel-weighting algorithm on the electrical recording led to a further 5% increase in SNR, to $\sigma_V \hat{=}$ 4.0 mV, and did not require adjustment of scaling and offset (Fig. 2d).

We imaged the dynamics of action potentials with sub-cellular resolution (Supplementary Fig. 5). To improve the signal-to-noise ratio we averaged multiple temporally registered movies of single spikes (Fig. 2e and Supplementary Movie 3). Action potentials appeared to occur nearly simultaneously throughout most regions of the cell, as expected given the field of view (100 μm) and exposure time (2 ms). However, in localized regions the action potential lagged by 2–3 ms. The pixel-weighting algorithm did not detect the cellular regions with delayed action potentials, but the lag is readily seen in Supplementary Movie 3. The present results suggest that Arch may be used to map intracellular dynamics of action

potentials in genetically specified neurons, in a manner similar to a recent demonstration with voltage sensitive dyes[12].

We created a gallery of single-trial optical and electrical recordings (Fig. 2f). At a 2 kHz frame rate, the signal-to-noise ratio in the fluorescence (spike amplitude:baseline noise) was 10.5. A spike-finding algorithm correctly identified 99.6% of the spikes (based on comparison to simultaneously recorded membrane potential), with a false-positive rate of 0.7% (n = 269 spikes; Online Methods). The average action potential waveform determined by fluorescence coincided with the waveform recorded electrically. Single cells were observed for up to 4 minutes of cumulative exposure, with no detectable change in resting potential or spike frequency.

We developed a procedure to electrically tag a single cell in an otherwise overgrown field of neurons, similar to that of Ref. 22. The average fluorescence of the population of cells, all expressing Arch, did not show clearly resolved cellular structures (Fig. 2g). A whole-cell patch was formed on one cell, which was then subjected to a voltage clamp triangle wave of amplitude 150 mV, under video observation. The weight matrix, indicating which pixels contained information about the applied voltage, yielded a clear image of the target cell and its processes. Electrical tagging provides a complement to genetic [23] and chemical [24] methods which are currently used to label single neurons.

In the absence of added retinal, neurons expressing Arch showed clearly identifiable fluorescence flashes accompanying individual spikes (Supplementary Fig. 6a), indicating that neurons contained sufficient endogenous retinal to populate some of the protein. Addition of supplemental retinal led to a 30 – 60% increase in fluorescence over 30 minutes (Supplementary Fig. 6b). Experiments with Arch and other microbial rhodopsins *in vivo* have shown that endogenous retinal is sufficient for optogenetic control of neural activity [25]. Thus Arch may function as a voltage indicator *in vivo* without exogenous retinal.

Arch(D95N) is a non-pumping voltage indicator

Illumination at 640 nm was far from the peak of the Arch absorption spectrum (λ = 558 nm), but the imaging laser nonetheless induced photocurrents of 10 – 20 pA in HEK cells expressing Arch (Fig. 3a). We sought to develop a mutant which did not perturb the membrane potential, yet which maintained voltage sensitivity. The mutation D85N in bacteriorhodopsin eliminated proton pumping [26], so we introduced the homologous mutation, D95N, into Arch. This mutation eliminated the photocurrent (Fig. 3a) and shifted several other photophysical properties of importance to voltage sensing (Table 1, Fig. 3, and Supplementary Fig. 7). Arch(D95N) was more sensitive to voltage than Arch and displayed a 3-fold increase in fluorescence between −150 mV and +150 mV, with nearly linear sensitivity from −120 to +120 mV, but had a slower response (Fig. 3b–d; Supplementary Movies 4 – 5). After calibration with a voltage ramp, Arch(D95N) resolved voltage steps of 10 mV, with a noise in the voltage estimated from fluorescence of 260 μV $Hz^{-1/2}$ over timescales < 12 s.

Under illumination conditions typically used for imaging neural activity (I = 1,800 W cm^{-2}, λ = 640 nm), the light-induced outward photocurrent was typically 10 pA in neurons

expressing Arch. Under current-clamp conditions this photocurrent shifted the resting potential of the neurons by up to −20 mV. For neurons near their activation threshold, this photocurrent could suppress firing (Fig. 4a), so we explored the non-pumping variant D95N as a voltage indicator in neurons. Illumination of Arch(D95N) did not perturb membrane potential in neurons (Fig. 4b).

Arch(D95N) reported neuronal action potentials on a single-trial basis (Fig. 4c). The response to a depolarizing current pulse was dominated by the slow component of the step response; yet the fast component of the response was sufficient to indicate action potentials. Efforts are underway to identify a non-pumping mutant with speed comparable to Arch.

Discussion

A comparison of Arch and Arch(D95N) to other fluorescent voltage indicators, plotted according to sensitivity and response speed is given in Fig. 5. Data and references are in Supplementary Table 1. The positions of existing indicators are approximate and obtained from literature data. The most sensitive fluorescent proteins, the VSFP 2.× family, have changes in fluorescence of approximately 10% per 100 mV of voltage, with a response time of approximately 100 ms. The SPARC family of voltage sensors has a 1 ms response time, and shows a fluorescence change of less than 1% per 100 mV. Microbial rhodopsin-based indicators (yellow region) are notably more sensitive than other probes. The most sensitive microbial rhodopsin-based indicator is PROPS, but PROPS only functions in prokaryotes[14]. Fluorescent voltage sensitive dyes have enabled optical recording of action potentials in brain slice with signal-to-noise exceeding that of Arch[12, 27], though phototoxicity and challenges with delivery prevent widespread use.

Arch is one of approximately 5,000 known microbial rhodopsins [28]. We suggest that this family of proteins should be explored for its ability to label biological membranes with a color-tunable, photostable, and environmentally sensitive chromophore, with no homology to GFP. The fluorescence and voltage-sensing properties of microbial rhodopsins are orthogonal to their native biological function, suggesting that these properties can be improved through minor changes to the protein sequence. Screens of wild-type and mutated microbial rhodopsins will be essential for identifying variants that are fast, like Arch, but that lack pumping, like Arch(D95N). Efforts to increase the brightness or to find other non-fluorescent imaging modalities are also of paramount importance. Initial efforts to observe two-photon fluorescence from Arch were not successful; but the excitation of Arch is red-shifted relative to most two-photon fluorophores so additional studies with spectrally tuned two-photon excitation are warranted. Simultaneous imaging of fluorescence from Arch and eGFP in a fusion protein may enable ratiometric voltage measurements, with improved robustness to variations in expression level or to movement, relative to single-band measurements. Care will be needed to avoid artifacts from environmental and statistical noise in the reference channel, as well as from differential photobleaching. Fusions with other fluorescent indicator proteins may enable simultaneous measurements of voltage and pH or Ca^{2+}. We expect the combination of optogenetic voltage measurement with the recently established techniques of optogenetic voltage control[29] to enable progress toward all-optical electrophysiology.

Methods

Protein constructs and membrane fractionation

All experiments were performed with an Arch-eGFP fusion. A lentiviral backbone plasmid encoding Arch-eGFP (FCK:Arch-EGFP, accession number BAA09452) was used to clone the Arch gene into the pet28b vector using the restriction sites EcoRI and NcoI. The D95N mutation was created separately in the pet28b and FCK backbones, using the QuikChangeII kit (Agilent) and the same DNA primers for both backbones (Supplementary Table 2).

Arch and its D95N mutant were expressed in *E. coli*, following Ref. [31]. Briefly, *E. coli* (strain BL21, pet28b plasmid) was grown in 1 L of LB with 100 μg mL^{-1} kanamycin, to an O.D. 600 of 0.4 at 37 °C. All-*trans* retinal (5 μM) and inducer (IPTG 0.5 mM) were added and cells were grown for an additional 3.5 hours in the dark. Cells were harvested by centrifugation and resuspended in 50 mM Tris, 2 mM $MgCl_2$ at pH 7.3 and lysed with a tip sonicator for 5 minutes. The lysate was centrifuged and the pellet was resuspended in PBS supplemented with 1.5% dodecyl maltoside (DM). The mixture was homogenized with a glass and teflon Potter Elvehjem homogenizer and centrifuged again. The solubilized protein in the supernatant was used for experiments.

Spectroscopic characterization of Arch and Arch(D95N)

The absorption spectra of fractionated *E. coli* membranes containing Arch and Arch(D95N) were determined using an Ocean Optics USB4000 spectrometer with a DT-MINI-2-GS light source (Supplementary Fig. 1). The peak extinction coefficients of microbial rhodopsins vary across rhodopsin types from 48,000 to 63,000 M^{-1} cm^{-1}.[30, 32–34] Due to the high homology between Arch and bacteriorhodopsin (BR), we used the BR extinction coefficient, 63,000 M^{-1} cm^{-1}, for Arch. The differing wavelengths of maximum absorption of Arch (558 nm) and Arch(D95N) (585 nm) led to different extinction coefficients at 633 nm, as shown in Table 1. For Arch, 633 nm was in the tail of the absorption while for Arch(D95N) 633 nm lay half way down the shoulder. The relative extinction coefficients of Arch and Arch(D95N) at 633 nm are independent of our choice to use BR as the reference for the peak extinction coefficient. Absorption spectra for Arch and Arch(D95N) were measured as a function of pH between pH 6 and 11.

The fluorescence emission spectra of Arch and Arch(D95N) were determined using illumination with a 100 mW, 532 nm laser (Dragon Lasers, 532GLM100) or a 25 mW, 633 nm HeNe laser (Spectra-Physics) (Supplementary Fig. 1). Scattered laser light was blocked with a 532 nm Raman notch filter (Omega Optical, XR03) or a 710/100 emission filter (Chroma), and fluorescence was collected perpendicular to the illumination with a 1,000 micron fiber, connected to an Ocean Optics QE65000 spectrometer. Spectra were integrated for 2 seconds. Arch and Arch(D95N) both had emission maxima at 687 nm. We do not know why the two proteins have such different peak absorption wavelengths but the same peak emission wavelength.

The fluorescence quantum yields of Arch and Arch(D95N) were determined by comparing the integrated emission intensity to emission of a sample of the dye Alexa 647 (Invitrogen). Briefly, the concentrations of micromolar solutions of dye and protein were determined

using a visible absorption spectrum. We used the extinction coefficients of 270,000 $M^{-1}cm^{-1}$ for Alexa 647 and 63,000 $M^{-1}cm^{-1}$ for Arch and Arch(D95N), assuming that these microbial rhodopsins have the same extinction coefficient as bacteriorhodopsin. The dye solution was then diluted 1:1,000 to yield a solution with comparable fluorescence emission to Arch. The fluorescence emission spectra of dye and protein samples were measured with 633 nm excitation. The quantum yield was then determined by the formula

$$QY_{Arch} = \frac{Fl_{Arch}}{Fl_{Alexa}} * \frac{\varepsilon_{Alexa}}{\varepsilon_{Arch}} * \frac{c_{Alexa}}{c_{Arch}} * QY_{Alexa}$$

where *Fl* is the integrated fluorescence from 660 to 760 nm, ε is the extinction coefficient at 633 nm and *c* is the concentration.

Relative photostability of Arch and eGFP

To perform a direct comparison of photostability of Arch and eGFP we studied the photobleaching of the Arch-eGFP fusion. This strategy guaranteed a 1:1 stoichiometry of the two fluorophores, simplifying the analysis. The experiments were performed on permeabilized cells, in the microscope, with video recording as the cells photobleached. We first recorded a movie of photobleaching of Arch under 640 nm illumination; then on the same field of view we recorded photobleaching of eGFP under 488 nm illumination, with illumination intensity adjusted to yield approximately the same initial count rate as for Arch. Fluorescence background levels were obtained from nearby protein-free regions of each movie and were subtracted from the intensity of the protein-containing regions. The area under each photobleaching timetrace was calculated, yielding an estimate of the total number of detected photons from each fluorophore. The eGFP emission (λ_{max} = 509 nm) and the Arch emission (λ_{max} = 687 nm) were collected through different emission filters, so the raw counts were corrected for the transmission spectra of the filters and the wavelength-dependent quantum yield of the EMCCD camera. The result was that the relative number of photons emitted prior to photobleaching for eGFP:Arch was 3.9:1, and for eGFP: Arch(D95N) this ratio was 10:1.

HEK cell culture

HEK-293 cells were grown at 37 °C, 5% CO_2, in DMEM supplemented with 10% FBS and penicillin-streptomycin. Plasmids were transfected using Lipofectamine and PLUS reagent (Invitrogen) following the manufacturer's instructions, and assayed 48–72 hours later. The day before recording, cells were re-plated onto glass-bottom dishes (MatTek) at a density of ~5,000 cells cm^{-2}.

The concentration of endogenous retinal in the HEK cells was not known, so the cells were supplemented with retinal by diluting stock retinal solutions (40 mM, DMSO) in growth medium to a final concentration of 5 μM, and then placing the cells back in the incubator for 1 – 3 hours. All imaging and electrophysiology were performed in Tyrode buffer (containing, in mM: 125 NaCl, 2 KCl, 3 $CaCl_2$, 1 $MgCl_2$, 10 HEPES, 30 glucose pH 7.3, and adjusted to 305–310 mOsm with sucrose). Only HEK cells having reversal potentials between −10 and −40 mV were included in the analysis.

Microscopy

Simultaneous fluorescence and whole-cell patch clamp recordings were acquired on a home-built, inverted epifluorescence microscope, operated at room temperature. Here we summarize the design considerations; a detailed specification is given in Supplementary Fig. 2. A key challenge was to collect fluorescence with high efficiency, while also achieving a large enough field of view to image an entire neuron and its processes. Typically, microscope objectives offer a tradeoff between magnification and light-gathering capacity (numerical aperture), which we sought to avoid. Additionally, we wanted the ability to change magnification while maintaining a patch on a single cell. The vibrations associated with switching objectives—particularly water or oil immersion objectives—are incompatible with simultaneous patch clamp. Finally, we wanted the capability to split the field of view into two wavelength bands, and to change magnification without changing the registration of the two halves of the image.

To achieve these goals simultaneously, we designed our microscope around a 60× NA 1.45 oil immersion objective (Olympus 1-U2B616), with variable zoom camera lenses to change illumination area and magnification. The magnification was continuously variable between 10 × and 66 ×, without touching the objective. The microscope readily converted between single-band and dual-band imaging, with only minor realignment.

On an upright electrophysiology setup retrofitted with a laser and EMCCD camera, a dipping objective (Olympus LUMPlanFl – 40 × W/IR; NA 0.8) collected enough light to record voltage-dependent fluorescence of HEK cells. However, recording of action potentials with high signal-to-noise ratio required a high NA objective (e.g. Olympus 1-U2B893 60 × Water NA 1.2; or 1-U2B616 60 × Oil NA 1.45).

Electrophysiology

Filamented glass micropipettes (WPI) were pulled to a tip resistance of 3–10 MΩ fire polished, and filled with internal solution (containing, in mM: 125 Potassium gluconate, 8 NaCl, 0.6 $MgCl_2$, 0.1 $CaCl_2$, 1 EGTA, 10 HEPES, 4 Mg-ATP, 0.4 Na-GTP, pH 7.3; adjusted to 295 mOsm with sucrose). The micropipettes were positioned with a Burleigh PCS 5000 micromanipulator. Whole-cell, voltage clamp recordings were acquired using an AxoPatch 200B amplifier (Molecular Devices), filtered at 2 kHz with the internal Bessel filter, and digitized with a National Instruments PCIE-6323 acquisition board at 10 kHz. Ambient 60 Hz noise was removed using a HumBug Noise Eliminator (AutoMate Scientific). For experiments requiring rapid modulation of transmembrane potential, series resistance and whole-cell capacitance were predicted to 95% and corrected to ~50%. Electrical stimuli were generated using the PCIE-6323 acquisition board and sent to the AxoPatch, which then applied these signals in either constant current or constant voltage mode.

Measurements of photocurrents were performed on HEK cells held in voltage clamp at 0 mV while being exposed to brief (200 ms) pulses of illumination at 640 nm at an intensity of 1,800 W cm^{-2}.

All experiments were performed at 24 °C.

Ramp and step-response of Arch and Arch(D95N)

To measure fluorescence as a function of membrane potential, a triangle wave was applied, with amplitude from −150 mV to +150 mV and period 12 s, with video recording at 100 ms per frame. A pixel weight matrix was calculated according to Eq. 2 (below) and applied to the movie images to generate a fluorescence number for each frame. These fluorescence values were divided by their minimum value (at $V = -150$ mV). The result is plotted as a function of V in Figs. 2 – 3. This procedure preferentially weighted data from pixels at the cell membrane, but did not entail any background subtraction. Comparable results were obtained by manually selecting pixels corresponding to a region of plasma membrane, and plotting their intensity as a function of V, without background subtraction. Background subtraction from the raw fluorescence would have yielded considerably larger values of ΔF/F.

The step response was measured in a similar manner, except that test waveforms consisted of a series of voltage pulses, from −70 mV to +30 mV with duration 300 ms and period 1 s. Cells were subjected to 20 repetitions of the waveform, and the fluorescence response was averaged over all iterations.

Frequency-dependent response functions of Arch and Arch(D95N)

Test waveforms consisted of a concatenated series of sine waves, each of duration 2 s, amplitude 100 mV, zero mean, and frequencies uniformly spaced on a logarithmic scale between 1 Hz and 1 kHz (31 frequencies total). The waveforms were discretized at 10 kHz and applied to the cell, while fluorescence movies were acquired at a frame rate of 2 kHz.

The model parameters for extracting $\hat{V_{FL}}(t)$ were calculated from the fluorescence response to low frequency voltages. These parameters were then used to calculate an estimated voltage at all frequencies.

The applied voltage was downsampled to 2 kHz to mimic the response of a voltage indicator with instantaneous response. For each applied frequency, the Fourier transform of $\hat{V_{FL}}(t)$ was calculated and divided by the Fourier transform of the downsampled $V(t)$. The amplitude of this ratio determined the response sensitivity. It was crucial to properly compensate pipette resistance and cell membrane capacitance to obtain accurate response spectra. Control experiments on cells expressing membrane-bound GFP showed no voltage-dependent fluorescence.

The power spectrum of $\hat{V_{FL}}(t)$ under constant $V = 0$ was also measured to enable calculations of signal-to-noise ratio for any applied $V(t)$.

Estimates of membrane potentials from fluorescence images

A common practice in characterizing fluorescent voltage indicators is to report a value of ΔF/F per 100 mV of membrane potential. We feel that this parameter is of limited use, for several reasons. First, the value of ΔF/F is highly sensitive to the method of background subtraction, particularly for indicators in which F approaches zero at some voltage. Second, ΔF/F contains no information about signal-to-noise ratio, which depends on absolute

fluorescence levels, background, and membrane targeting of the indicator. Third, the ratio ΔF/F contains no information about the temporal stability of the fluorescence. Fluctuations may arise due to intracellular transport, photobleaching, or other photophysics. Fourth, definitions of absolute fluorescence are often subjective, depending on a user-defined Region of Interest which might or might not include pieces of internal membranes or other cells.

We therefore sought a measure of the performance of a voltage indicator which reported the information content of the fluorescence signal. We sought an algorithm to infer membrane potential from a series of fluorescence images. We used the accuracy with which the estimated membrane potential matched the true membrane potential (as reported by patch clamp recording) as a measure of indicator performance. The algorithm described below is implemented in our analysis (Supplementary Software).

The estimated membrane potential, $\hat{V_{FL}}(t)$, was determined from the fluorescence in two steps. First we trained a model relating membrane potential to fluorescence at each pixel. We used the highly simplified model that the fluorescence signal, $S_i(t)$, at pixel i and time t, is given by:

$$S_i(t)=a_i+b_iV(t)+\varepsilon_i(t), \quad [1]$$

where a_i and b_i are position-dependent but time-independent constants, the membrane potential $V(t)$ is time-dependent but position independent, and $\varepsilon_i(t)$ is spatially and temporally uncorrelated Gaussian white noise with pixel-dependent variance:

$$\left\langle \varepsilon_i(t_1)\varepsilon_j(t_2)\right\rangle =\sigma_i^2\delta_{i,j}\delta(t_1-t_2),$$

where $\langle\ \rangle$ indicates an average over time.

This model neglects nonlinearity in the fluorescence response to voltage, finite response time of the protein to a change in voltage, photobleaching, cell-motion or stage drift, and the fact that if $\varepsilon_i(t)$ is dominated by shot-noise then its variance should be proportional to $S_i(t)$, and its distribution should be Poisson, not Gaussian. Despite these simplifications, the model of Eq. 1 provided good estimates of membrane potential when calibrated from the same dataset to which it was applied.

The pixel-specific parameters in Eq. 1 are determined by a least-squares procedure, as follows. We define the deviations from the mean fluorescence and mean voltage by

$$\delta S_i(t)=S_i(t)-\left\langle S_i(t)\right\rangle$$
$$\delta V(t)=V(t)-\left\langle V(t)\right\rangle .$$

Then the estimate for the slope $\hat{b_i}$ is: $\hat{b}_i=\frac{\left\langle \delta S_i\delta V\right\rangle}{\left\langle \delta V^2\right\rangle}$, and the offset is:

$$\hat{a}_i = \left\langle S_i \right\rangle - \hat{b}_i \left\langle V \right\rangle .$$

A pixel-by-pixel estimate of the voltage is formed from:

$$\hat{V}_i(t) = \frac{S_i(t)}{\hat{b}_i} - \frac{\hat{a}_i}{\hat{b}_i}.$$

The accuracy of this estimate is measured by

$$\varsigma_i^2 = \left\langle \left(\hat{V}_i(t) - V(t) \right)^2 \right\rangle .$$

A maximum likelihood weight matrix is defined by:

$$w_i \equiv \frac{1/\varsigma_i^2}{\sum_i 1/\varsigma_i^2}. \quad [2]$$

This weight matrix favors pixels whose fluorescence is an accurate estimator of voltage in the training set.

To estimate the membrane potential, the pixel-by-pixel estimates are combined according to:

$$\hat{V}_{FL}(t) = \sum_i w_i \hat{V}_i(t) \quad [3]$$

Within the approximations underlying Eq. 1, Eq. 3 is the maximum likelihood estimate of $V(t)$.

In cases where the membrane potential is not known, one can replace $V(t)$ by the total intensity of the entire image $I(t)$, provided that there is only a single cell with varying membrane potential within the image. In this case, the algorithm preferentially weights pixels whose intensity co-varies with the mean intensity. Such pixels are associated with the membrane. This modified procedure yields an estimate of the underlying intensity variations in the membrane. The output resembles the true membrane potential, apart from an unknown offset and scale factor. A key feature of this modified procedure is that it enables spike identification without a patch pipette.

On a video record of 30,000 frames taken (e.g. 30 s of data at 1,000 frames s^{-1}), the training phase of the algorithm took approximately 3 min to run on a desktop PC. Application of the weighting coefficients to incoming video data could be performed in close to real time. Small shifts in the field of view due to stage drift or bumps of the apparatus are compensated by using image registration techniques to translate the pixel weight map. Large changes in focus or movement to a new field of view required re-training of the algorithm.

Molecular biology and virus production

Plasmids encoding Arch-EGFP (FCK:Arch-EGFP) were either used directly for experiments in HEK cells, or first used to produce VSVg-pseudotyped virus according to published methods[16]. For pseudotyping, HEK-293 cells were co-transfected with pDelta 8.74, VSVg, and either of the Arch backbone plasmids using Lipofectamine and PLUS reagent (Invitrogen). Viral supernatants were collected 48 hours later and filtered using a 0.45 μm membrane. The virus medium was used to infect neurons without further concentration.

The D95N mutation was introduced using the QuickChange kit (Stratagene), according to the manufacturer's instructions using the same primers as the *E. coli* plasmid.

Neuronal cell culture

E18 rat hippocampi (BrainBits) were mechanically dissociated in the presence of 1 mg mL^{-1} papain (Worthington) before plating at 5,000 – 30,000 cells per dish on poly-L-lysine and Matrigel-coated (BD Biosciences) glass-bottom dishes. At this density synaptic inputs did not generate spontaneous firing. Cells were incubated in N+ medium (100 mL Neurobasal medium, 2 mL B27 supplement, 0.5 mM glutamine, 25 μM glutamate, penicillin-streptomycin) for 3 hours. An additional 300 μL virus medium was added to the cells and incubated overnight, then brought to a final volume of 2 mL N+ medium. After two days, cells were fed with 1.5 mL N+ medium. Cells were fed with 1 mL N+ medium without glutamate at 4 DIV, and fed 1 mL every 3–4 days after. Cells were allowed to grow until 10–14 DIV. Cells were supplemented with retinal by diluting stock retinal solutions (40 mM, DMSO) in growth medium to a final concentration of 5 μM, and then placing the cells back in the incubator for 1 – 3 hours, after which they were used for experiments.

Whole-cell current clamp recordings were obtained from mature neurons under the same conditions used for HEK cells recordings. Series resistance and pipette capacitance were corrected. Only neurons having resting potentials between −50 and −70 mV were used in the analysis.

Spike sorting

We used a simple spike identification algorithm that could be applied either to electrically recorded $V(t)$ or to optically determined $V(\hat{t})$. The input trace was convolved with a reference spike. Sections of the convolved waveform that crossed a user-defined threshold were identified as putative spikes. Multiple spikes that fell within 10 ms (a consequence of noise-induced glitches near threshold) were clustered and identified as one.

Supplementary Material

Refer to Web version on PubMed Central for supplementary material.

Acknowledgments

We thank F. Engert (Harvard University) for generously providing support to ADD, providing laboratory space during the early stages of this work, and for facilitating this collaboration. We thank E. Boyden (Massachusetts Institute of Technology), K. Rothschild (Boston University), and A. Ting (Massachusetts Institute of Technology) for discussions and contributions of equipment and reagents. We also thank G. Lau, B. Lilley, and H. Inada for

technical assistance. This work was supported by the Harvard Center for Brain Science, NIH grants 1-R01-EB012498-01 and New Innovator grant 1-DP2-OD007428, the Harvard/MIT Joint Research Grants Program in Basic Neuroscience, an Intelligence Community Postdoctoral Fellowship (JK), a National Science Foundation Graduate Fellowship (DH), a Helen Hay Whitney Postdoctoral Fellowship (AD), and Charles A. King Trust Postdoctoral Fellowship (AD). The data reported in this paper are tabulated in the Supporting Online Material and are available upon request.

References

1. Cohen LB, Keynes RD, Hille B. Light scattering and birefringence changes during nerve activity. Nature. 1968; 218:438–441. [PubMed: 5649693]
2. Tasaki I, Watanabe A, Sandlin R, Carnay L. Changes in fluorescence, turbidity, and birefringence associated with nerve excitation. Proc. Natl. Acad. Sci. U. S. A. 1968; 61:883–888. [PubMed: 4301149]
3. Peterka DS, Takahashi H, Yuste R. Imaging Voltage in Neurons. Neuron. 2011; 69:9–21. [PubMed: 21220095]
4. Akemann W, Mutoh H, Perron A, Rossier J, Knopfel T. Imaging brain electric signals with genetically targeted voltage-sensitive fluorescent proteins. Nat. Methods. 2010; 7:643–649. [PubMed: 20622860]
5. Scanziani M, Hausser M. Electrophysiology in the age of light. Nature. 2009; 461:930–939. [PubMed: 19829373]
6. Homma R, et al. Wide-field and two-photon imaging of brain activity with voltage-and calcium-sensitive dyes. Philosophical Transactions of the Royal Society B: Biological Sciences. 2009; 364:2453.
7. Jiang J, Yuste R. Second-Harmonic Generation Imaging of Membrane Potential with Photon Counting. Microscopy and Microanalysis. 2008; 14:526–531. [PubMed: 18986606]
8. Tsutsui H, Karasawa S, Okamura Y, Miyawaki A. Improving membrane voltage measurements using FRET with new fluorescent proteins. Nat. Meth. 2008; 5:683–685.
9. Siegel MS, Isacoff EY. A Genetically Encoded Optical Probe of Membrane Voltage. Neuron. 1997; 19:735–741. [PubMed: 9354320]
10. Sjulson L, Miesenbock G. Rational optimization and imaging in vivo of a genetically encoded optical voltage reporter. J. Neurosci. 2008; 28:5582. [PubMed: 18495892]
11. Bradley J, Luo R, Otis TS, DiGregorio DA. Submillisecond Optical Reporting of Membrane Potential In Situ Using a Neuronal Tracer Dye. J. Neurosci. 2009; 29:9197–9209. [PubMed: 19625510]
12. Popovic MA, Foust AJ, McCormick DA, Zecevic D. The spatio-temporal characteristics of action potential initiation in layer 5 pyramidal neurons: a voltage imaging study. J. Physiol. 2011; 589:4167–4187. [PubMed: 21669974]
13. Tian L, et al. Imaging neural activity in worms, flies and mice with improved GCaMP calcium indicators. Nat. Meth. 2009; 6:875–881.
14. Kralj JM, Hochbaum DR, Douglass AD, Cohen AE. Electrical spiking in Escherichia coli probed with a fluorescent voltage indicating protein. Science. 2011; 333:345–348. [PubMed: 21764748]
15. Ihara K, et al. Evolution of the archaeal rhodopsins: evolution rate changes by gene duplication and functional differentiation. J. Mol. Biol. 1999; 285:163–174. [PubMed: 9878396]
16. Chow BY, et al. High-performance genetically targetable optical neural silencing by light-driven proton pumps. Nature. 2010; 463:98–102. [PubMed: 20054397]
17. Lanyi JK. Bacteriorhodopsin. Annu. Rev. Physiol. 2004; 66:665–688. [PubMed: 14977418]
18. Kolodner P, Lukashev EP, Ching Y, Rousseau DL. Electric-field-induced Schiff-base deprotonation in D85N mutant bacteriorhodopsin. Proc. Nat. Acad. Sci. U. S. A. 1996; 93:11618–11621.
19. Lenz MO, et al. First steps of retinal photoisomerization in proteorhodopsin. Biophys. J. 2006; 91:255–262. [PubMed: 16603495]
20. Shaner NC, Steinbach PA, Tsien RY. A guide to choosing fluorescent proteins. Nat. Meth. 2005; 2:905.

21. Mukamel EA, Nimmerjahn A, Schnitzer MJ. Automated analysis of cellular signals from large-scale calcium imaging data. Neuron. 2009; 63:747–760. [PubMed: 19778505]
22. Borst A, Heck D, Thomann M. Voltage signals of individual Purkinje cell dendrites in rat cerebellar slices. Neurosci. Lett. 1997; 238:29–32. [PubMed: 9464647]
23. Livet J, et al. Transgenic strategies for combinatorial expression of fluorescent proteins in the nervous system. Nature. 2007; 450:56–62. [PubMed: 17972876]
24. Novikova L, Novikov L, Kellerth JO. Persistent neuronal labeling by retrograde fluorescent tracers: a comparison between Fast Blue, Fluoro-Gold and various dextran conjugates. J. Neurosci. Methods. 1997; 74:9–15. [PubMed: 9210570]
25. Boyden ES, Zhang F, Bamberg E, Nagel G, Deisseroth K. Millisecond-timescale, genetically targeted optical control of neural activity. Nat. Neurosci. 2005; 8:1263–1268. [PubMed: 16116447]
26. Tittor J, Schweiger U, Oesterhelt D, Bamberg E. Inversion of proton translocation in bacteriorhodopsin mutants D85N, D85T, and D85, 96N. Biophys. J. 1994; 67:1682–1690. [PubMed: 7819500]
27. Obaid AL, Salzberg BM. Optical Recording of Electrical Activity in Guinea-pig Enteric Networks Using Voltage-sensitive Dyes. J. Vis. Exp. 2009; 34
28. Venter JC, et al. Environmental genome shotgun sequencing of the Sargasso Sea. Science. 2004; 304:66–74. [PubMed: 15001713]
29. Fenno L, Yizhar O, Deisseroth K. The development and application of optogenetics. Annu. Rev. Neurosci. 2011; 34:389–412. [PubMed: 21692661]
30. Rehorek M, Heyn MP. Binding of all-trans-retinal to the purple membrane. Evidence for cooperativity and determination of the extinction coefficient. Biochemistry (N, Y.). 1979; 18:4977–4983.
31. Bergo V, Spudich EN, Spudich JL, Rothschild KJ. Conformational changes detected in a sensory rhodopsin II-transducer complex. J. Biol. Chem. 2003; 278:36556–36562. [PubMed: 12821665]
32. Scharf B, Hess B, Engelhard M. Chromophore of sensory rhodopsin II from Halobacterium halobium. Biochemistry (N, Y.). 1992; 31:12486–12492.
33. Oesterhelt D, Meentzen M, Schuhmann L. Reversible Dissociation of the Purple Complex in Bacteriorhodopsin and Identification of 13 - cis and all - trans - Retinal as its Chromophores. European Journal of Biochemistry. 1973; 40:453–463. [PubMed: 4781385]
34. Vogeley L, et al. Crystal structure of the Anabaena sensory rhodopsin transducer. J. Mol. Biol. 2007; 367:741–775. [PubMed: 17289074]

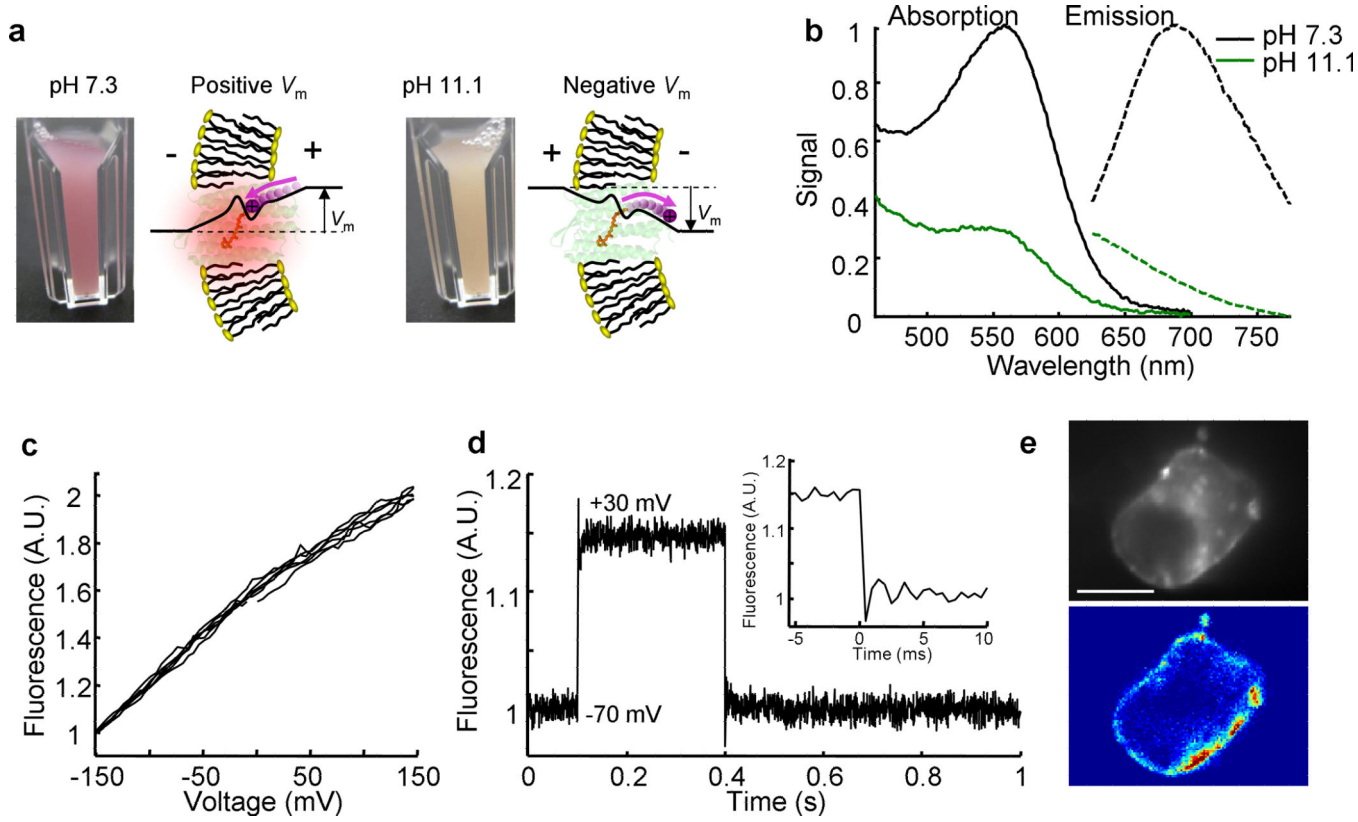

Figure 1.

Arch is a fluorescent voltage indicator. (**a**) Model of Arch as a voltage sensor, in which pH and membrane potential can both alter the protonation of the Schiff base. The cuvettes contain intact *E. coli* expressing Arch. (**b**) Absorption (solid line) and fluorescence emission (dashed line) spectra of Arch at neutral and high pH. (**c**) Fluorescence of Arch as a function of membrane potential. The fluorescence was divided by its value at −150 mV. (**d**) Dynamic response of Arch to steps in membrane potential between −70 mV and +30 mV. The overshoots on the rising and falling edges were an artifact of electronic compensation circuitry. The smaller amplitude compared to (**c**) is because background subtraction was not performed in (**d**). Data averaged over 20 cycles. Inset: Step response occurred in less than the 500 μs resolution of the imaging system. (**e**) Top: HEK cell expressing Arch, visualized via Arch fluorescence. Bottom: pixel-weight matrix showing regions of voltage-dependent fluorescence. Scale bar 10 μm.

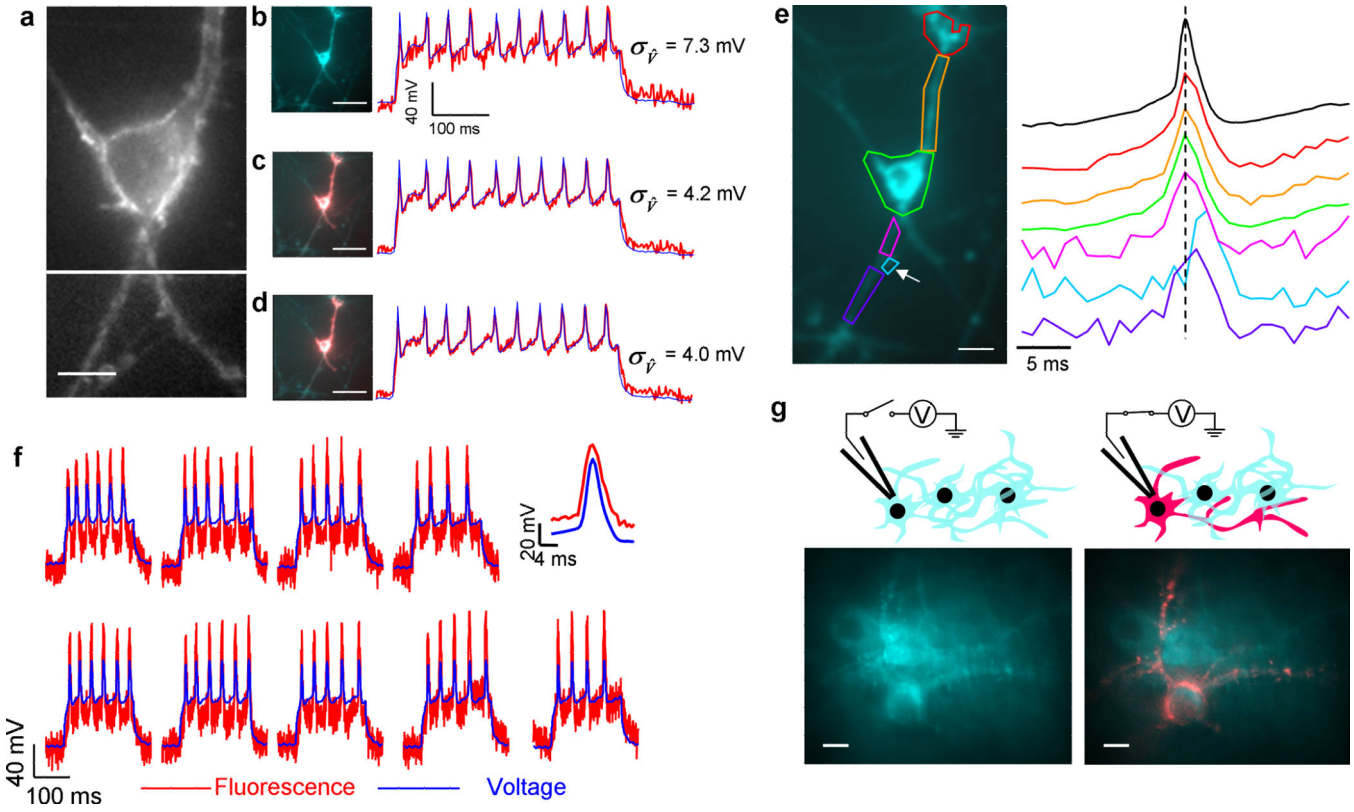

Figure 2.

Optical recording of action potentials with Arch. (**a**) Cultured rat hippocampal neuron imaged via fluorescence of Arch (composite of two fields of view). Scale bar 10 μm. (**b**) Left: Low-magnification image of neuron in (**a**). Right: Whole-field fluorescence (red) during a single-trial recording at 500 frames s^{-1}. The fluorescence was scaled to overlay on the electrical recording (blue). (**c**) Left: Pixel-by-pixel map of cross-correlation between whole-field and single-pixel intensities (red) overlaid on the average fluorescence (cyan). Note that the process extending to the top left of the cell body does not appear in the red channel; it is electrically decoupled from the cell. Right: Pixel-weighted fluorescence (red) and electrical recording (blue). (**d**) Left: Pixel-by-pixel map of cross-correlation between electrical recording and single-pixel intensities (red) overlaid on the average fluorescence (cyan). Right: Pixel-weighted fluorescence (red) and electrical recording (blue). Scale bar in (**b**) – (**d**) 50 μm. (**e**) Sub-cellular localization of an action potential. Left: regions of interest indicated by colored polygons. Right: time-course of an action potential averaged over 98 events in the regions indicated with the corresponding colors. The top black trace is the electrical recording. Optical recordings appear broadened due to the finite (2 ms) exposure time of the camera. The white arrow indicates a small protrusion that has a substantially delayed AP relative to the rest of the cell. Vertical scale on fluorescence traces is arbitrary. Scale bar 10 μm. (**f**) Gallery of single-trial recordings of action potentials recorded at a frame rate of 2 kHz. The pixel weight matrix was determined from the accompanying electrophysiology recording. Top right: Averaged spike response for 269 events in a single cell, showing voltage (blue) and fluorescence (red). (**g**) Identification of processes associated with a single target neuron in a dense culture. Left: Time-average Arch fluorescence of

multiple transfected neurons. Right: Membrane potential was modulated by whole-cell voltage clamp. Responsive pixels were identified via cross-correlation of pixel intensity and applied voltage (red). Scale bar 10 μm.

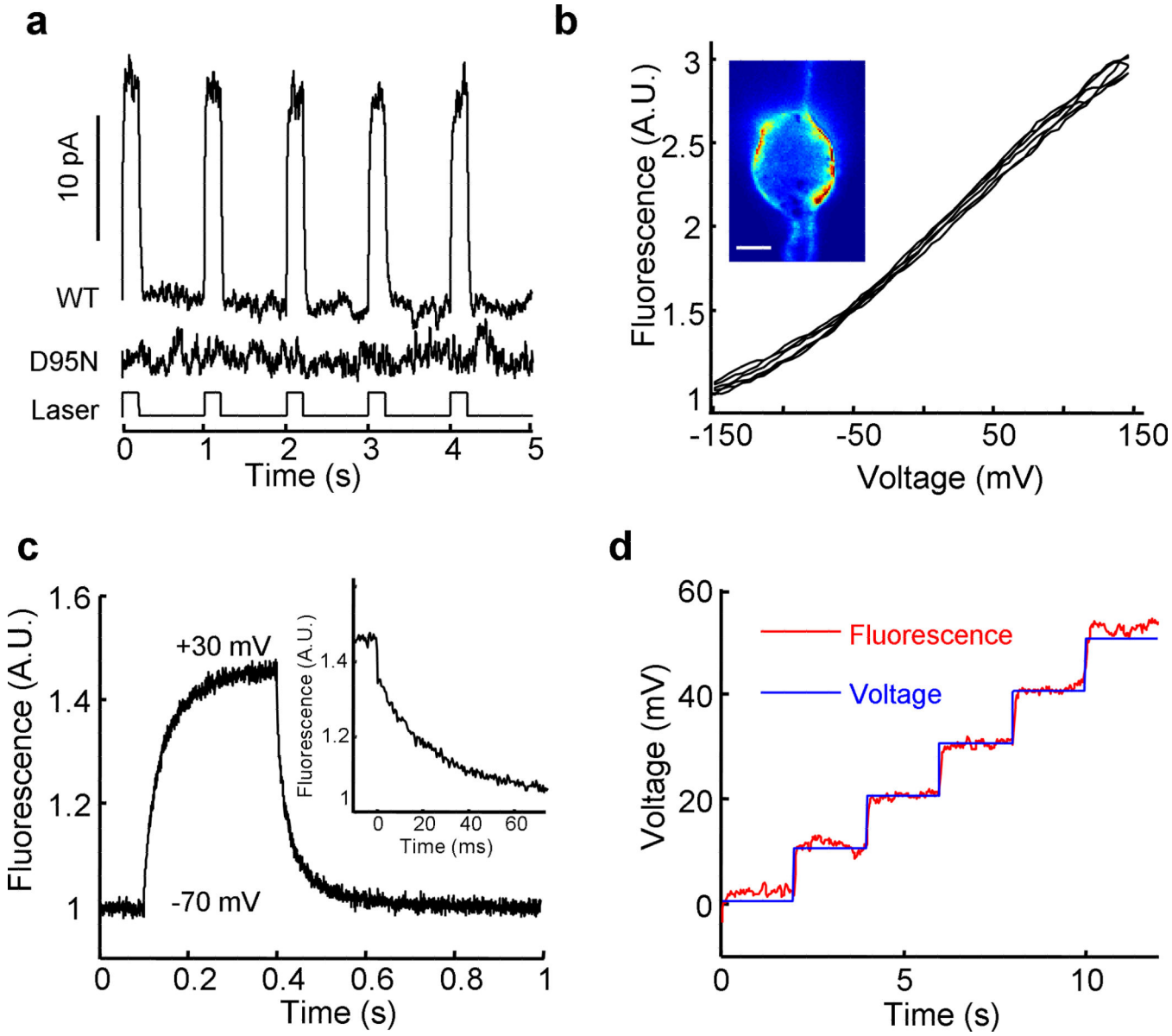

Figure 3.

Arch(D95N) shows voltage-dependent fluorescence but no photocurrent. (**a**) Photocurrents in Arch and Arch(D95N), expressed in HEK cells clamped at $V = 0$. Cells were illuminated with pulses of light ($\lambda = 640$ nm; $I = 1{,}800$ W cm^{-2}). (**b**) Fluorescence of Arch(D95N) as a function of membrane potential.. Inset: map of voltage sensitivity. Scale bar 5 μm. (**c**) Dynamic response of Arch(D95N) to steps in membrane potential between −70 mV and +30 mV. Data averaged over 20 cycles. Inset: Step response comprised a component faster than 500 μs (20% of the response) and a component with a time constant of 41 ms. (**d**) Response of Arch(D95N) to 10 mV steps in membrane potential.

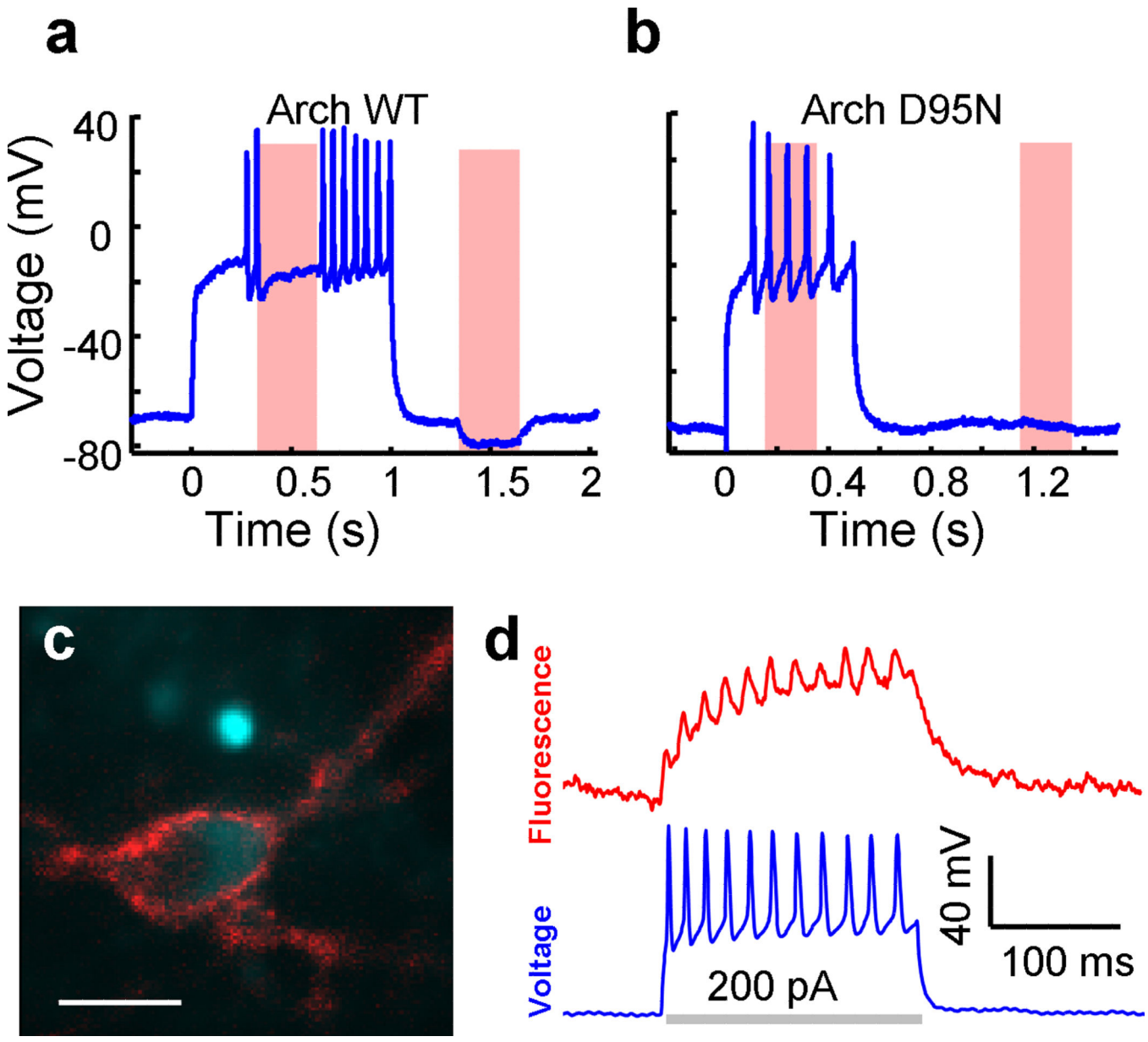

Figure 4.

Optical recording of action potentials with Arch(D95N). (**a**) Electrically recorded membrane potential of a neuron expressing Arch, subjected to pulses of current injection and laser illumination. Red bars indicate laser illumination. (**b**) Same as (**a**) in a neuron expressing Arch(D95N). (**c**) Neuron expressing Arch(D95N), showing Arch(D95N) fluorescence (cyan), and regions of voltage-dependent fluorescence (red). Scale bar 10 μm. (**d**) Single-trial recording of whole-cell membrane potential (blue) and weighted Arch(D95N) fluorescence (red) during a train of action potentials.

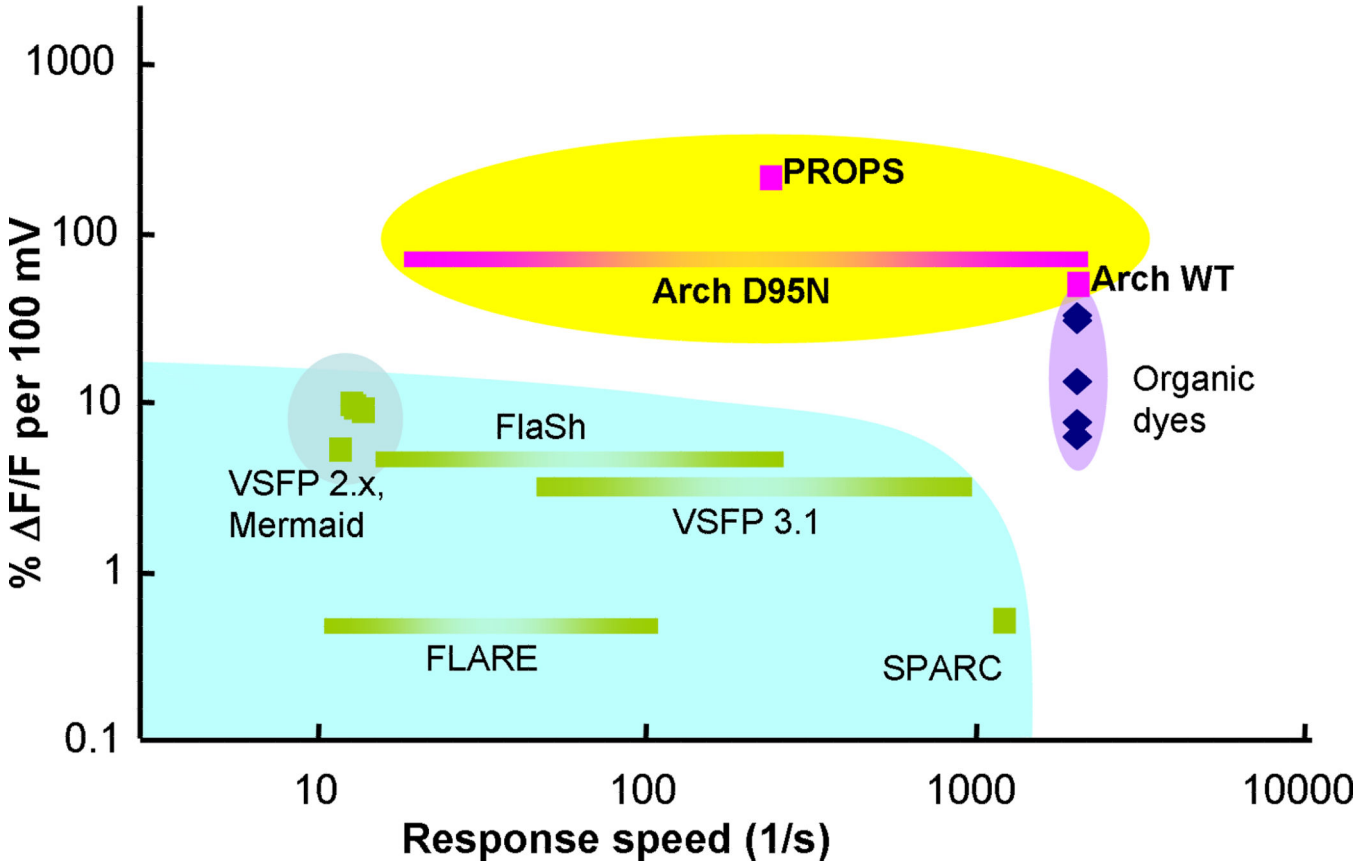

Figure 5.

Optical indicators of membrane potential classified by speed and sensitivity. Green marks represent indicators based on fusions of GFP homologues to membrane proteins. Pink marks represent indicators based on microbial rhodopsins. Blue diamonds represent organic dyes and hybrid dye-protein indicators. Extended bars denote indicators where two time constants have been reported. The Proteorhodopsin Optical Proton Sensor (PROPS) is homologous to Arch(D95N), but only functions in bacteria. The speeds of most organic dyes are not known precisely; however they respond in less than 500 μs.

Table 1

Optical and electrical response of Arch and Arch(D95N).

	λ_{max} abs (nm)	λ_{max} em[1] (nm)	ε_{633} [2] ($M^{-1}cm^{-1}$)	QY [3]	Photostability relative to eGFP[4]	pK_a of SB [5]	$\tau_{response}$ [6] (ms)	Noise in $\hat{V_{FL}}$ [7] ($\mu V\ Hz^{-1/2}$)	Photo-current
Arch	558	687	6,300	9×10^{-4}	0.25	10.1	< 0.5	625	yes
Arch(D95N)	585	687	37,500	4×10^{-4}	0.1	8.9	41	260	no

[1] Excitation at λ = 532 nm.

[2] Absorption spectra calibrated assuming the same peak extinction coefficient as Bacteriorhodopsin, 63,000 M^{-1} cm^{-1} (Ref. 30; see Online Methods).

[3] Determined via comparison to Alexa 647 with excitation at λ = 633 nm.

[4] Measured in a 1:1 fusion with eGFP.

[5] Determined via singular value decomposition on absorption spectra.

[6] Determined from step-response. Arch(D95N) has a minor component of its response (20%) that is fast (< 500 μs).

[7] $\hat{V_{FL}}$ is the membrane potential estimated from fluorescence. Noise determined at frequencies $f \geq 0.1$ Hz in HEK cells.